Zeolites

International Edition: DOI: 10.1002/anie.201813533
German Edition: DOI: 10.1002/ange.201813533

Preferential Siting of Aluminum Heteroatoms in the Zeolite Catalyst Al-SSZ-70

*Zachariah J. Berkson, Ming-Feng Hsieh, Stef Smeets, David Gajan, Alicia Lund, Anne Lesage, Dan Xie, Stacey I. Zones, Lynne B. McCusker, Christian Baerlocher, and Bradley F. Chmelka**

Abstract: *The adsorption and reaction properties of heterogeneous zeolite catalysts (e.g. for catalytic cracking of petroleum, partial oxidation of natural gas) depend strongly on the types and distributions of Al heteroatoms in the aluminosilicate frameworks. The origins of these properties have been challenging to discern, owing in part to the structural complexity of aluminosilicate zeolites. Herein, combined solid-state NMR and synchrotron X-ray powder diffraction analyses show the Al atoms locate preferentially in certain framework sites in the zeolite catalyst Al-SSZ-70. Through-covalent-bond 2D $^{27}Al\{^{29}Si\}$ J-correlation NMR spectra allow distinct framework Al sites to be identified and their relative occupancies quantified. The analyses show that 94% of the Al atoms are located at the surfaces of the large-pore interlayer channels of Al-SSZ-70, while only 6% are in the sub-nm intralayer channels. The selective siting of Al atoms accounts for the reaction properties of catalysts derived from SSZ-70.*

Nanoporous zeolites are of considerable technological interest because of their high surface areas, well-defined sub-nanometer pore dimensions, and exchangeable cations.[1] Their molecular adsorption or reaction sites enable important industrial applications, including air–gas separations[2] and heterogeneous catalysis of reactions such as hydrocarbon conversions[3] and reduction of nitric oxides for automotive pollution mitigation.[4] Aluminosilicate zeolites are composed of corner-sharing SiO_4 and AlO_4 tetrahedra, where the AlO_4 tetrahedra are associated with catalytically active sites when the excess negative framework charges are balanced by acidic countercations, such as H^+. The molecular diffusion, adsorption, and reaction properties of zeolite catalysts are strongly influenced by the nanopore dimensions, the framework architectures, and the types and distributions of heteroatom sites (e.g. Al) and the associated cations. Understanding and controlling heteroatom locations in zeolite catalysts have been severely limited by the non-stoichiometric substitution of heteroatoms into the framework and their distributions, which are challenging to characterize. Determining such distributions in different zeolite frameworks and correlating their macroscopic adsorption and/or catalytic reaction properties has been a long-standing challenge in the understanding of zeolite catalysts.

Heteroatom distributions in zeolites have long been recognized to depend strongly on synthesis conditions, including the compositions of the precursor materials and organic and inorganic structure-directing cations.[5] Information on heteroatom distributions in zeolites has been accessed previously by using several scattering or spectroscopic techniques. For example, the relative positions and proximities of Al atoms and their associated cations may be identified by deconvolution of infrared or ultraviolet-visible spectra of zeolite frameworks,[6–8] though such spectra are generally poorly resolved. While the similar electron densities of Al and Si atoms make them challenging to distinguish using scattering techniques,[9] Al occupancies in different tetrahedral (T) sites have been determined for large single crystals by synchrotron X-ray standing-wave diffraction.[10] For as-synthesized zeolites containing organic structure-directing agents (OSDAs) that drive preferential configurations of heteroatom sites, information on framework heteroatom distributions may be extracted by the refinement of synchrotron X-ray diffraction data.[11–13] Heteroatom distributions in zeolites can be influenced in favorable cases by the substitution of Al for B[14] or the careful selection of OSDAs and synthesis conditions.[11,15–17]

Herein, analyses of solid-state two-dimensional (2D) NMR spectra with complementary synchrotron X-ray powder diffraction analyses establish the preferential siting of Al heteroatoms in calcined zeolite Al-SSZ-70. The layered zeolite SSZ-70 has recently emerged as a promising platform

[*] Dr. Z. J. Berkson, Dr. M.-F. Hsieh, Dr. L. B. McCusker, Dr. C. Baerlocher, Prof. Dr. B. F. Chmelka
Department of Chemical Engineering
University of California
Santa Barbara, CA 93106 (USA)
E-mail: bradc@engineering.ucsb.edu
Dr. S. Smeets, Dr. L. B. McCusker, Dr. C. Baerlocher
Laboratory of Crystallography, ETH Zurich
Vladimir-Prelog-Weg 5, 8093 Zurich (Switzerland)
Dr. D. Gajan, Dr. A. Lund, Dr. A. Lesage
Institut des Sciences Analytiques UMR 5280 (CNRS/Université Lyon 1/ENS Lyon), Université Lyon, Centre de RMN à Très Hauts Champs
69100 Villeurbanne (France)
Dr. D. Xie, Dr. S. I. Zones
Chevron Energy Technology Company
Richmond, CA 94802 (USA)
Dr. M.-F. Hsieh
Present address: Johnson Matthey Technology Centre
Chilton P.O. Box 1, Belasis Avenue, Billingham TS23 1LB (UK)
Dr. S. Smeets
Present address: Kavli Institute of Nanoscience, Delft University of Technology
Van der Maasweg 9, 2629 HZ Delft (The Netherlands)

Supporting information (experimental details, 2D ^{27}Al MQMAS analyses, 1D ^{27}Al and ^{29}Si NMR spectra, NMR sensitivity enhancement under low-temperature conditions, additional discussion) and the ORCID identification number(s) for the author(s) of this article can be found under: https://doi.org/10.1002/anie.201813533.

for new catalysts because it can be exfoliated to generate high-surface-area active materials that exhibit enhanced catalysis rates for alkylation reactions,[18] while calcined Al-SSZ-70 exhibits high catalytic activity for hydrocarbon cracking.[19] The structure of calcined SSZ-70 has 14 crystallographically distinct T sites.[20] SSZ-70 crystallizes into hexagonal flakes (Figure 1 a) and has two types of 2-dimensional

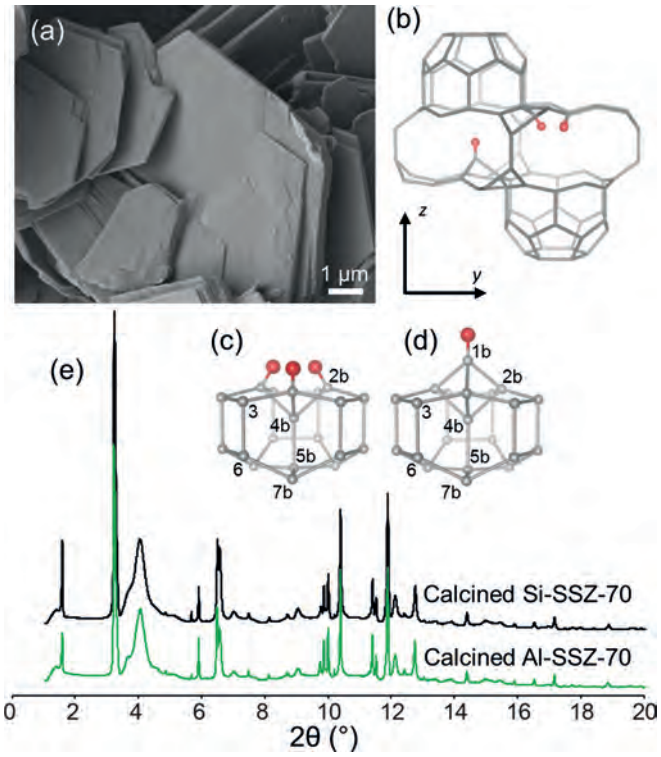

Figure 1. a) SEM image of Al-SSZ-70. b) Interlayer structure of calcined SSZ-70, showing the two types of interlayer -OH species (red; (c,d)). e) Synchrotron XRPD patterns of calcined Si- (black) and Al-SSZ-70 (green).

channel systems with effective cross-sectional pore openings of 4.4×5.9 Å^2 (within the **MWW**-type layers) and 4.0×11.5 Å^2 (between the **MWW**-type layers). However, in contrast to other **MWW**-type zeolite catalysts, the catalytic selectivity of calcined Al-SSZ-70 for hydrocarbon cracking does not change substantially with time on stream,[19] characteristic of reactions occurring in a single type of nanochannel system.[21] Calcined SSZ-70 exhibits two types of silanol species that protrude into the interlayer channels (Figure 1 b): "nests" of three closely spaced silanols (Figure 1 c) and isolated silanols (Figure 1 d). The different T sites in SSZ-70 differ with respect to their covalent bonding configurations and positions relative to the inter- and intralayer channel surfaces. For example, T1a,b, T2a,b, and T3 are at the surfaces of the interlayer channels, while T5a,b, T6, T7a,b, and T8a,b are at the surfaces of the intralayer channels. Al heteroatoms located in such different T sites are expected to exhibit distinct adsorption and reaction properties. The synchrotron X-ray powder diffraction (XRPD) patterns of calcined Si- and Al-SSZ-70 are virtually identical (Figure 1 e), indicating that the long-range ordering of T-atoms in SSZ-70 is indistinguishable in silicate and aluminosilicate forms, despite their different compositions.

Analyses of the 1D ^{29}Si MAS NMR spectra (Figure S1 in the Supporting Information) show that the local environments of framework ^{29}Si atoms in calcined SSZ-70 are almost identical in the siliceous and aluminosilicate forms. Because of the small absolute quantity of Al in the material (Si/Al = 25, Ref. [19]) and overlapping ^{29}Si NMR signals from different Q^4(0Al) and Q^3(0Al) species in SSZ-70,[20] the ^{29}Si signals from Q^4(1Al) species cannot be resolved or quantified from the 1D ^{29}Si MAS NMR spectra alone. (The $Q^m(n\text{Al})$ notation refers to a tetrahedrally coordinated ^{29}Si atom that is covalently linked through bridging O atoms to m other Si or Al atoms, of which n are Al.)

Solid-state ^{27}Al NMR spectroscopy is sensitive to the local environments of the crucial Al heteroatoms in zeolite frameworks and is in principle capable of distinguishing between ^{27}Al species in different T sites in aluminosilicate zeolites.[22] However, the resolution of such spectra is often limited owing to strong quadrupolar interactions of ^{27}Al ($I = 5/2$) nuclei, as well as inhomogeneous distributions of ^{27}Al species. The resolution of solid-state ^{27}Al NMR spectra can be improved by using high magnetic fields (> 18 Tesla) and 2D NMR techniques.[23] For example, high-field ^{27}Al multiple-quantum magic-angle-spinning (MQMAS) NMR analyses of different samples of aluminosilicate zeolite ZSM-5, which has 24 crystallographically distinct T sites, have led to the identification and assignment of at least 12 different ^{27}Al signals associated with different T sites.[24–26] In addition, recent 2D ^{27}Al{^{29}Si} dipolar-mediated NMR analyses of ZSM-5 provided evidence of Al incorporation into 4 of the 24 T sites,[27] although through-space dipolar interactions can manifest signal intensities from next-nearest neighbor T sites and non-covalently bonded moieties that reduce resolution. General methods for determining the distributions and relative populations of Al heteroatoms in zeolites have been elusive, particularly for materials of high catalytic importance that often exhibit exceptional structural complexity, such as Al-SSZ-70.

Herein, we report the preferential siting of Al heteroatoms in 5 of the 14 T sites in calcined Al-SSZ-70 established by analyses of solid-state 2D NMR heteronuclear correlation spectra,[27,28] which resolve distinct signals from different framework ^{27}Al moieties and provide direct evidence for the incorporation of Al atoms into specific sites. The 1D and 2D ^{27}Al MAS NMR spectra of calcined Al-SSZ-70 in Figure 2 show well-resolved ^{27}Al signals at 60 ppm, 55 ppm, and 49 ppm from ^{27}Al atoms in tetrahedrally coordinated environments, as well as a signal at −5 ppm from octahedrally coordinated ^{27}Al species. The relatively narrow (2–3 ppm full-width half-maximum, fwhm) ^{27}Al signals suggest that the ^{27}Al heteroatoms are sited in specific T sites, rather than being randomly distributed.

Specific locations of Al heteroatoms in calcined Al-SSZ-70 are determined by identification of the nearest-neighbor ^{29}Si sites to which the different ^{27}Al species are covalently bonded. This is achieved by measuring 2D ^{27}Al{^{29}Si} heteronuclear multiple quantum correlation (HMQC) NMR spectra,[29–31] which here correlate the shifts of ^{27}Al-O-^{29}Si spin

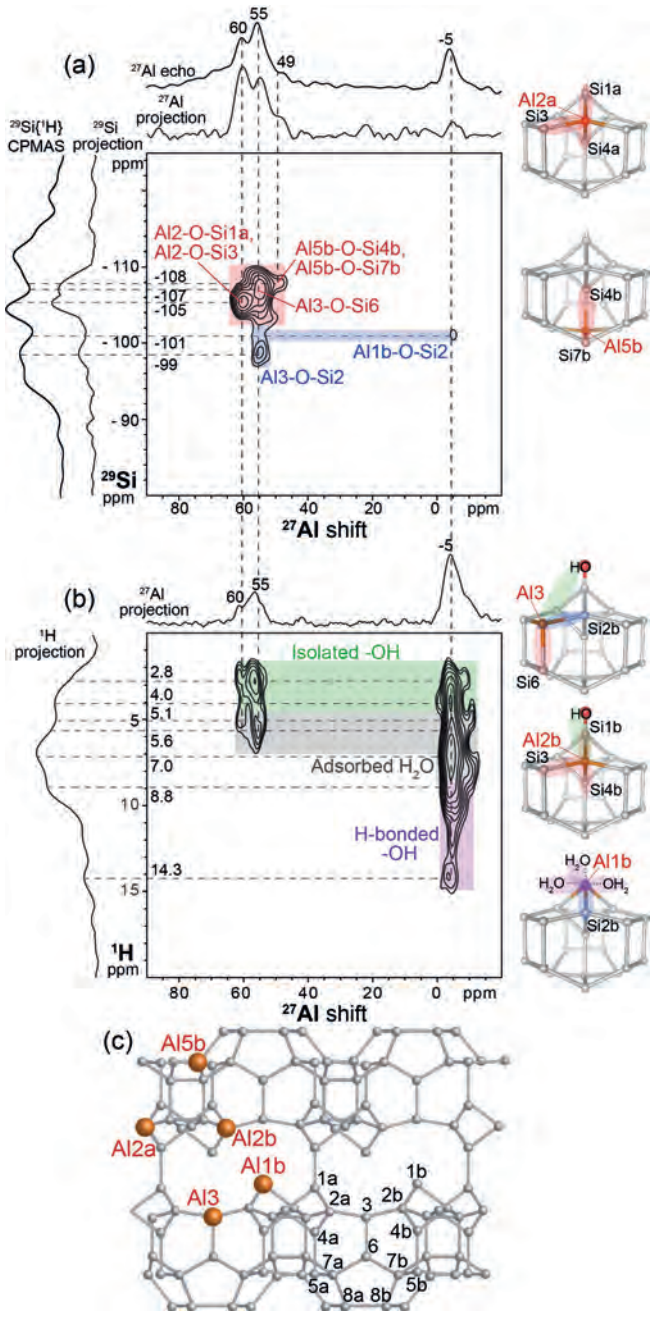

Figure 2. Solid-state 2D a) ^{27}Al{^{29}Si} *J*-HMQC and b) ^{27}Al{^{1}H} HETCOR NMR spectra of calcined Al-SSZ-70 acquired at 18.8 Tesla, 10 kHz MAS, and 97 K. Solid-state 1D ^{27}Al echo and ^{29}Si{^{1}H} CPMAS spectra acquired under the same conditions are shown along the corresponding axes for comparison with the 1D projections of the 2D spectra. The accompanying insets show the *J*-coupling between ^{27}Al atoms (orange) and ^{29}Si atoms (gray) at nearest-neighbor T sites consistent with the correlated intensities in the 2D spectra in (a) and (b). c) Schematic diagram of the framework structure of Al-SSZ-70, with orange indicating the T sites that are occupied by Al heteroatoms as determined by the solid-state NMR analyses.

pairs and are mediated by through-covalent-bond $J_{\text{Al-Si}}$ couplings.[32] Acquisition of such spectra has been exceptionally challenging in the past, but is enabled here by the use of low-temperature (< 100 K) measurement conditions, which lead to improved NMR signal sensitivity (ca. 5× increase) (Figure S2, S3). For example, the 2D ^{27}Al{^{29}Si} *J*-HMQC spectrum of calcined Al-SSZ-70 in Figure 2a shows correlated signal intensities at ^{27}Al shifts of 60 ppm, 55 ppm, and 49 ppm that are correlated with ^{29}Si signals in the chemical shift range −105 ppm to −108 ppm (red band in Figure 2a) from different Q^4(1Al) ^{29}Si species. The ^{27}Al signal at 55 ppm is additionally correlated with ^{29}Si signals in the −99 to −101 ppm range (blue band), which also arise from Q^4(1Al) species. The different correlated ^{27}Al-^{29}Si signals in the 2D ^{27}Al{^{29}Si} *J*-mediated spectrum in Figure 2a are assigned based on comparisons with previous 2D ^{29}Si{^{29}Si} and ^{29}Si{^{1}H} NMR analyses of calcined Si-SSZ-70,[20] analyses of 2D ^{27}Al MQMAS spectra of Al-SSZ-70 (Figures S4, S5, Tables S1, S2), well-established semi-empirical correlations relating the isotropic ^{27}Al and ^{29}Si chemical shift values to the -T-O-T- bond angles,[33–35] and prior literature.[36] The predicted and experimental isotropic ^{27}Al and ^{29}Si chemical shifts associated with different T sites in calcined Al-SSZ-70 are compared in Figure S6. On the basis of isotropic ^{29}Si chemical shift values calculated for Q^4(1Al) species in each T site (Table S3), the correlated signals at −99 to −101 ppm in the ^{29}Si dimension (blue band in Figure 2a) are assigned to framework Al-O-Si2 Q^4(1Al) moieties, while those at −105, −107, and −108 ppm (red band; Figure 2a) are assigned, respectively, to Al-O-Si3 and Al-O-Si1a, Al-O-Si6, and Al-O-Si4b and Al-O-Si7b Q^4(1Al) moieties. The correlated ^{27}Al-^{29}Si signals at 60, 55, and 49 ppm in the ^{27}Al dimension must therefore arise from ^{27}Al species that are covalently bonded (through bridging O atoms) to Si1a and Si3, Si6 and Si2, and Si4b and Si7b Q^4(1Al) species, respectively. The positions of the ^{27}Al heteroatoms are further constrained by analysis of the isotropic ^{27}Al chemical shifts determined by 2D ^{27}Al MQMAS analyses at different magnetic field strengths and temperatures (Figures S4, S5), which are compared with the calculated values for ^{27}Al atoms in each T site (Table S2, Figure S6). With the constraints provided by the 2D ^{27}Al{^{29}Si} *J*-mediated correlation spectrum, these analyses enable the ^{27}Al signals at 60, 55, and 49 ppm to be confidently assigned to fully crosslinked Al2a/b, Al3, and Al5b sites, respectively. The unambiguous identification of the different ^{27}Al-O-^{29}Si connectivities enables the specific locations of Al heteroatoms to be established, even for a complex zeolite, such as Al-SSZ-70.

Interestingly, octahedrally coordinated ^{27}Al species are also located within the aluminosilicate zeolite framework. Octahedrally coordinated framework ^{27}Al species in aluminosilicate zeolites are generally associated with framework defect sites and/or partial dealumination of the framework.[37] The correlation of the ^{29}Si signal at −101 ppm from Si2 Q^4(1Al) species and the ^{27}Al signal at −5 ppm (blue band, Figure 2a) establishes that the octahedrally coordinated ^{27}Al species in Al-SSZ-70 are in fact covalently linked to Si2 Q^4(1Al) species and are therefore in T1a/b or T3 sites. The presence of this weak correlated signal is confirmed by the 2D ^{27}Al{^{29}Si} *J*-HMQC spectrum acquired at 9.4 Tesla and 91 K (Figure S7). Because of steric hindrance near framework T1a and T3 sites, the presence of octahedrally coordinated Al1a or Al3 species is considered unlikely. By comparison, T1b is a partially crosslinked site that protrudes into the interlayer

channels, where ^{27}Al atoms could coordinate to adsorbed water and/or -OH groups. Octahedrally coordinated Al1b species are therefore expected to be associated with significant hydrogen bonding.

Strong H-bonds associated with the octahedrally coordinated ^{27}Al species in calcined Al-SSZ-70 are identified by analysis of the 2D ^{27}Al{^{1}H} heteronuclear correlation (HETCOR) spectrum of calcined Al-SSZ-70 (Figure 2b). The spectrum manifests correlated ^{27}Al{^{1}H} signal intensities from ^{27}Al-^{1}H nuclear spin pairs that are dipole–dipole coupled through space, being principally sensitive to interactions over distances of < 5 Å.[38] Analyses of 1D ^{1}H and 2D ^{29}Si{^{1}H} HETCOR NMR spectra of calcined Si- and Al-SSZ-70 (Figures S3, S8) show that both materials possess isolated and strongly H-bonded interlayer -OH species. The 2D ^{27}Al{^{1}H} HETCOR spectrum of calcined Al-SSZ-70 in Figure 2b shows correlated intensities at 55 and 60 ppm in the ^{27}Al dimension and at 2.8–4.0 ppm (green band, Figure 2b) and 5.1–5.6 ppm (gray band, Figure 2b) in the ^{1}H dimension, which arise from tetrahedrally coordinated ^{27}Al species proximate to isolated interlayer -OH groups[20] and nanopore-adsorbed water,[39] respectively. These signals are consistent with the assignment of the ^{27}Al signals at 55 and 60 ppm to fully crosslinked Al2a/b and Al3 sites, respectively. By comparison, the ^{27}Al signal at -5 ppm is correlated with a broad, continuous distribution of ^{1}H signals from 2.8–14.3 ppm. The ^{1}H signals at 2.8–4.0 ppm (green band, Figure 2b) are assigned to isolated -OH species, those at 5.1–7.0 ppm (gray band, Figure 2b) to adsorbed water molecules, and those at 8.8–14.3 ppm (purple band, Figure 2b) to H-bonded -OH groups with -OH···O- distances of 2.5 Å to 2.8 Å as estimated from well-established semi-empirical correlations.[39,40] The correlated ^{27}Al{^{1}H} signal intensities thus establish that the octahedrally coordinated ^{27}Al species are in close proximities to isolated and strongly H-bonded -OH moieties. All of the solid-state NMR results are therefore consistent with the assignment of the ^{27}Al signal at -5 ppm to partially crosslinked Al1b sites, which are bonded (through bridging oxygen atoms) to three framework Si atoms and protrude into the interlayer channels, where Al atoms are able to adopt octahedral configurations by coordinating with water molecules or -OH groups.

Notably, the majority of the Al heteroatoms in calcined Al-SSZ-70 are located in framework sites at the surfaces of the interlayer channels. Based on the analyses of the solid-state 2D NMR spectra, each of the ^{27}Al signals can be assigned with confidence to an individual T site within the zeolite Al-SSZ-70 framework structure. Specifically, the ^{27}Al signals at 60, 55, and 49 ppm are assigned to ^{27}Al atoms in fully crosslinked T-sites 2a/b, 3, and 5b, respectively, while the ^{27}Al signal at -5 ppm is assigned to octahedrally coordinated ^{27}Al atoms in T-site 1b. Importantly, the relative occupancies of the ^{27}Al heteroatoms in these different SSZ-70 framework sites are not the same. In fact, they are very different. Their relative populations are quantified by deconvolution of the 1D single-pulse ^{27}Al spectrum (Figure S9), yielding the fractional occupancies of Al atoms in each of the five T sites (Table S4) that are shown in the schematic structure of calcined Al-SSZ-70 (Figure 2c). The great majority of the ^{27}Al species (94%) are in T2a/b, T3, or T1b sites, which are located at the surfaces of the interlayer channels. The remainder of the ^{27}Al species (6%) are at T5b sites, which are located at the surfaces of the intralayer channels.

Because of the different positions and local structures of Al atoms within the SSZ-70 framework, the different heteroatom sites are expected to influence the catalyst adsorption and reaction properties. The catalytic cracking of long-chain alkanes by Al-SSZ-70 is characteristic of a large-pore zeolite[19] rather than one with both large- and medium-pore channel systems, as might be expected from the structure of the zeolite. This is fully consistent with the preferential siting of Al heteroatoms at the surfaces of the large-pore interlayer channels, and indicates that the catalytic cracking (and probably other) reactions occur primarily there. The results also account for the high catalytic activities of catalysts derived from delamination of SSZ-70:[18,41] nearly all of the heteroatoms associated with the cation-exchange sites in Al-SSZ-70 are at the surfaces of the interlayer channels that are exposed upon exfoliation and therefore are accessible for post-synthetic modification and/or catalysis.

The locations of the majority of the Al heteroatoms at sites at the surfaces of the interlayer channels indicate that the bulky *N*,*N*′-diisobutylimidazolium cations used as OSDAs during zeolite synthesis direct the Al heteroatoms to specific sites in the Al-SSZ-70 framework. The roles of the OSDA in the preferential siting of Al heteroatoms in Al-SSZ-70 remain under investigation. In addition, the above analyses are expected to be useful for further studies on the structures of as-synthesized Al-SSZ-70 (Figure S10).

More broadly, recent research in zeolite materials has focused on generating active sites in specific regions of zeolites by designing zeolite architectures for specific reactions[16] or directing heteroatoms to targeted locations within a zeolite framework.[42] Such control over heteroatom locations is achievable in part for borosilicate zeolites by changing the OSDA and synthesis conditions.[13] However, similar capabilities have been lacking for aluminosilicate zeolites, in part because of the absence of experimental techniques that are capable of resolving Al occupancies at different T sites. The results reported here demonstrate that solid-state 2D NMR analyses, in combination with synchrotron XRPD, can establish Al locations and occupancies in complicated aluminosilicate zeolite frameworks like SSZ-70. This opens prospects for adjusting the Al distribution, and correspondingly the catalytic properties, by judicious selection of OSDAs and zeolite synthesis conditions.

In summary, the preferential siting of Al heteroatoms at 5 of the 14 T sites in calcined Al-SSZ-70 has been established by using 2D ^{27}Al{^{29}Si} and ^{27}Al{^{1}H} NMR correlation spectra to determine the T-site connectivities and hydration environments of specific ^{27}Al sites. The analyses show that the majority of Al heteroatoms in Al-SSZ-70 are located at the surfaces of the interlayer channel regions, which are expected to strongly influence the adsorption and catalytic reaction properties of the material. Such insights provide a deeper atomic-level understanding of the adsorption and reaction properties of this emerging catalytic material. The approach used is general and can be expected to provide similar

understanding for other heteroatom-containing zeolite catalysts, aiding in the future design of new catalytic materials with improved activity, selectivity, and stability.

Acknowledgements

This work was supported in part by the Chevron Energy Technology Company (Richmond, California, USA). The solid-state MAS NMR measurements at the University of California, Santa Barbara (UCSB), made use of the shared facilities of the UCSB MRL, supported by the MRSEC program of the NSF under Award No. DMR 1720256. Z.J.B. and B.F.C. thank the TGIR-RMN-THC Fr3050 CNRS for access to the 18.8 T DNP NMR facility at the CRMN and financial support was received from the EQUIPEX contract ANR-10-EQPX-47-01. S.S. acknowledges the Swiss National Science Foundation (Award No. 177761). We thank Drs. A. Cervellino and N. Casati for their assistance with the powder diffraction measurements on the Materials Science Beamline at the Swiss Light Source in Villigen, Switzerland.

Conflict of interest

The authors declare no conflict of interest.

Keywords: aluminum · NMR spectroscopy · solid acids · zeolites

How to cite: *Angew. Chem. Int. Ed.* **2019**, *58*, 6255 – 6259
Angew. Chem. **2019**, *131*, 6321 – 6325

[1] W. J. Roth, et al., *Nat. Chem.* **2013**, *5*, 628 – 633.
[2] B. Wang, A. P. Côté, H. Furukawa, M. O'Keeffe, O. M. Yaghi, *Nature* **2008**, *453*, 207 – 211.
[3] E. T. C. Vogt, B. M. Weckhuysen, *Chem. Soc. Rev.* **2015**, *44*, 7342 – 7370.
[4] C. Paolucci, et al., *Science* **2017**, *357*, 898 – 903.
[5] V. Gábová, J. Dědeček, J. Čejka, *Chem. Commun.* **2003**, 1196 – 1197.
[6] J. Dědeček, D. Kaucký, B. Wichterlová, O. Gonsiorová, *Phys. Chem. Chem. Phys.* **2002**, *4*, 5406 – 5413.
[7] R. Gounder, E. Iglesia, *J. Am. Chem. Soc.* **2009**, *131*, 1958 – 1971.
[8] J. Hun Kwak, H. Zhu, J. H. Lee, C. H. F. Peden, J. Szanyi, *Chem. Commun.* **2012**, *48*, 4758.
[9] J. Dědeček, Z. Sobalík, B. Wichterlová, *Catal. Rev. Sci. Eng.* **2012**, *54*, 135 – 223.
[10] J. A. van Bokhoven, T. L. Lee, M. Drakopoulos, C. Lamberti, S. Thie, J. Zegenhagen, *Nat. Mater.* **2008**, *7*, 551 – 555.
[11] A. B. Pinar, L. Gómez-Hortigüela, L. B. McCusker, J. Pérez-Pariente, *Chem. Mater.* **2013**, *25*, 3654 – 3661.
[12] S. Smeets, L. B. McCusker, C. Baerlocher, D. Xie, C. Y. Chen, S. I. Zones, *J. Am. Chem. Soc.* **2015**, *137*, 2015 – 2020.
[13] S. Smeets, L. B. McCusker, C. Baerlocher, S. Elomari, D. Xie, S. I. Zones, *J. Am. Chem. Soc.* **2016**, *138*, 7099 – 7106.
[14] S. I. Zones, A. Benin, S.-J. Hwang, D. Xie, S. Elomari, M.-F. Hsieh, *J. Am. Chem. Soc.* **2014**, *136*, 1462 – 1471.
[15] J. R. Di Iorio, C. T. Nimlos, R. Gounder, *ACS Catal.* **2017**, *7*, 6663 – 6674.
[16] E. M. Gallego, M. T. Portilla, C. Paris, A. León-Escamilla, M. Boronat, M. Moliner, A. Corma, *Science* **2017**, *355*, 1051 – 1054.
[17] K. Muraoka, W. Chaikittisilp, Y. Yanaba, T. Yoshikawa, T. Okubo, *Angew. Chem. Int. Ed.* **2018**, *57*, 3742 – 3746; *Angew. Chem.* **2018**, *130*, 3804 – 3808.
[18] R. C. Runnebaum, X. Ouyang, J. A. Edsinga, T. Rea, I. Arslan, S.-J. J. Hwang, S. I. Zones, A. Katz, *ACS Catal.* **2014**, *4*, 2364 – 2368.
[19] R. H. Archer, J. R. Carpenter, S.-J. Hwang, A. W. Burton, C.-Y. Chen, S. I. Zones, M. E. Davis, *Chem. Mater.* **2010**, *22*, 2563 – 2572.
[20] S. Smeets, Z. J. Berkson, D. Xie, S. I. Zones, W. Wan, X. Zou, M. F. Hsieh, B. F. Chmelka, L. B. McCusker, C. Baerlocher, *J. Am. Chem. Soc.* **2017**, *139*, 16803 – 16812.
[21] S. I. Zones, T. V. Harris, *Microporous Mesoporous Mater.* **2000**, *35 – 36*, 31 – 46.
[22] M. Haouas, F. Taulelle, C. Martineau, *Prog. Nucl. Magn. Reson. Spectrosc.* **2016**, *94 – 95*, 11 – 36.
[23] L. Frydman, D. M. Grant, R. K. Harris, *Encycl. Nucl. Magn. Reson.* **2002**, *9*, 262 – 274.
[24] S. Sklenak, J. Dědeček, C. Li, B. Wichterlová, V. Gábová, M. Sierka, J. Sauer, *Angew. Chem. Int. Ed.* **2007**, *46*, 7286 – 7289; *Angew. Chem.* **2007**, *119*, 7424 – 7427.
[25] S. Sklenak, J. Dědeček, C. Li, B. Wichterlová, V. Gábová, M. Sierka, J. Sauer, *Phys. Chem. Chem. Phys.* **2009**, *11*, 1237 – 1247.
[26] J. Holzinger, P. Beato, L. F. Lundegaard, J. Skibsted, *J. Phys. Chem. C* **2018**, *122*, 15595 – 15613.
[27] E. Dib, T. Mineva, E. Veron, V. Sarou-Kanian, F. Fayon, B. Alonso, *J. Phys. Chem. Lett.* **2018**, *9*, 19 – 24.
[28] A. G. M. Rankin, P. B. Webb, D. M. Dawson, J. Viger-Gravel, B. J. Walder, L. Emsley, S. E. Ashbrook, *J. Phys. Chem. C* **2017**, *121*, 22977 – 22984.
[29] A. Lesage, D. Sakellariou, S. Steuernagel, L. Emsley, *J. Am. Chem. Soc.* **1998**, *120*, 13194 – 13201.
[30] P. Florian, E. Veron, T. F. G. Green, J. R. Yates, D. Massiot, *Chem. Mater.* **2012**, *24*, 4068 – 4079.
[31] M. Valla, et al., *J. Am. Chem. Soc.* **2015**, *137*, 10710 – 10719.
[32] D. Massiot, et al., *C. R. Chim.* **2010**, *13*, 117 – 129.
[33] S. Ramdas, J. Klinowski, *Nature* **1984**, *308*, 521 – 523.
[34] E. Lippmaa, A. Samoson, M. Magi, *J. Am. Chem. Soc.* **1986**, *108*, 1730 – 1735.
[35] D. M. Dawson, R. F. Moran, S. E. Ashbrook, *J. Phys. Chem. C* **2017**, *121*, 15198 – 15210.
[36] M. A. Camblor, A. Corma, M.-J. Díaz-Cabañas, C. Baerlocher, *J. Phys. Chem. B* **1998**, *102*, 44 – 51.
[37] A. Omegna, J. A. van Bokhoven, R. Prins, *J. Phys. Chem. B* **2003**, *107*, 8854 – 8860.
[38] M. T. Janicke, C. C. Landry, S. C. Christiansen, D. Kumar, G. D. Stucky, B. F. Chmelka, *J. Am. Chem. Soc.* **1998**, *120*, 6940 – 6951.
[39] J. P. Yesinowski, H. Eckert, G. R. Rossman, *J. Am. Chem. Soc.* **1988**, *110*, 1367 – 1375.
[40] X. Xue, M. Kanzaki, *J. Am. Ceram. Soc.* **2009**, *92*, 2803 – 2830.
[41] M. Aigner, N. A. Grosso-Giordano, A. Okrut, S. Zones, A. Katz, *React. Chem. Eng.* **2017**, *2*, 842 – 851.
[42] S. I. Zones, C. Y. Chen, A. Benin, S.-J. Hwang, *J. Catal.* **2013**, *308*, 213 – 225.

Manuscript received: November 27, 2018
Version of record online: March 29, 2019

Angewandte Chemie
Eine Zeitschrift der Gesellschaft Deutscher Chemiker

Supporting Information

Preferential Siting of Aluminum Heteroatoms in the Zeolite Catalyst Al-SSZ-70

*Zachariah J. Berkson, Ming-Feng Hsieh, Stef Smeets, David Gajan, Alicia Lund, Anne Lesage, Dan Xie, Stacey I. Zones, Lynne B. McCusker, Christian Baerlocher, and Bradley F. Chmelka**

anie_201813533_sm_miscellaneous_information.pdf

Supporting Information

Table of Contents

1. Experimental section

Materials. The Al-SSZ-70 materials were synthesized according to the protocol described previously[1] using N,N-diisobutyl-imidazolium hydroxide as the organic structure-directing agent (OSDA). 6 mmol of tetraethyl orthosilicate (TEOS) and 0.25 mmol aluminum isopropoxide was added to a solution containing 3 mmol of diisobutyl-imidazolium hydroxide (from a 0.48 M solution) in a tared Teflon cup for a 23 ml Parr pressure reactor. The Si/Al ratio in the synthesis mixture was 24. The reagents were then kept in the closed cup for 2 days to allow for the hydrolysis of the metal esters to occur. The top was then taken off the cup and the cup was placed in a fume hood for the evaporation of the alcohol byproducts and some of the water while the mass loss was monitored to determine the water/silica ratio. After several days of evaporation, water was added to the cup to achieve the desired water/silica ratio of 7. Using a balance in a fume hood, 3 mmol of HF (from a 48 wt% HF solution) were carefully added dropwise. The reactor was then closed up and loaded onto a rotating spit (43 RPM) and heated to 150 °C for 1-2 weeks. The reaction progress was assessed every 7-10 days by extracting a small aliquot, washing the reaction product, and XRD analysis. The reaction rate may be increased up by providing seed crystallites (3% of overall silica content) from an all-silica synthesis conducted as this one but without the Al reagent.

After the phase purity of the Al SSZ-70 sample was confirmed by XRD analysis, the sample was loaded as a thin dispersion of powder into a thin Pyrex dish for calcination. The dish was loaded into a programmable convection-heated oven with an air flow of 20 SCFT air per minute. The material was heated at 1 °C/min up to 120 °C. It was maintained at that temperature for 2 h to remove as much water as possible. The temperature was then increased by 1 °C/min to 540 °C. The material was maintained at that temperature for 5 h and then allowed to slowly cool to room temperature in the oven. The mass loss from decomposition of the guest organic molecule is typically in the range of 15-18 wt%.[1] The Si/Al ratio in the final crystalline product is approximately 25.[1]

Characterization. Synchrotron XRPD data were collected on both calcined and as-synthesized samples of Al-SSZ-70 in a rotating 0.3 mm capillary on the MS-Powder beamline at the Swiss Light Source in Villigen, Switzerland (wavelength 0.70848 Å, MYTHEN II detector).[2]

Solid-state 1D and 2D MAS NMR spectroscopy was used to analyze the ^{1}H, ^{27}Al, and ^{29}Si environments in calcined Al-SSZ-70. The ^{1}H and ^{29}Si chemical shifts were referenced to tetramethylsilane (TMS) at 0.0 ppm, using tetrakis(trimethylsilyl)-silane as a secondary external reference. The ^{27}Al spin-lattice T_1 relaxation times were measured using saturation recovery experiments to be 40 ms or less at 295 K and 650 ms or less at 90-100 K for all of the ^{27}Al signals. The ^{27}Al shifts were referenced to a 0.5 M solution of $Al(NO_3)_3$ at 0.0 ppm as an external reference. The 1D single-pulse ^{27}Al and 2D ^{27}Al triple-quantum MAS (3QMAS) spectra measured at 295 K and 18.8 T were acquired on a Bruker AVANCE-III Ultrashield Plus 800 MHz (18.8 T) narrow-bore spectrometer operating at a Larmor frequency of 208.520 MHz for ^{27}Al and using a Bruker 2.5 mm broadband double-resonance H-X probehead. The 2D ^{27}Al 3QMAS spectrum in Fig. S4 was obtained at 35 kHz MAS, using 2400 transients, a repetition time of 0.1 s, an incremental t_1 step size of 14.29 μs, and 200 increments in the indirect isotropic dimension for a total acquisition time of 27 h. The 1D quantitative single-pulse ^{27}Al spectrum

was acquired using a 0.27 μs π/12 pulse, 512 transients, and a repetition time of 0.2 s. Low temperature MAS NMR conditions (<100 K) were used to improve NMR signal sensitivity and thereby enable the acquisition of 2D ^{27}Al{^{29}Si} heteronuclear multiple quantum correlation (HMQC) NMR spectra for materials with natural abundance ^{29}Si (4.7%), as discussed in Section 3 below. The 2D ^{27}Al{^{29}Si} *J*-HMQC and ^{27}Al{^{1}H} HETCOR spectra in Fig. 2 were acquired on a Bruker ASCEND 800 MHz (18.8 T) DNP NMR spectrometer operating at Larmor frequencies of 799.781, 208.387 and 158.864 for ^{1}H, ^{27}Al, and ^{29}Si, respectively, and equipped with a 3.2 mm triple-resonance HXY low-temperature MAS probehead. The 2D ^{27}Al{^{29}Si} *J*-HMQC spectrum was acquired with an experimentally-optimized τ delay of 14.4 ms to refocus the weak (<10 Hz) ^{27}Al-O-^{29}Si scalar *J* couplings, a repetition time of 2 s for each of 512 transients, 12.5 kHz MAS, a rotor-synchronized incremental t_1 step size of 80 μs, and 50 increments in the indirect ^{29}Si dimension for a total acquisition time of 14 h. The 2D ^{27}Al{^{1}H} heteronuclear correlation (HETCOR) spectrum in Figure 2b was acquired using homonuclear ^{1}H-^{1}H eDUMBO-1_{22} decoupling[4] during the ^{1}H evolution period, which yields narrower ^{1}H linewidths (2-3 ppm fwhm), compared to the 1D ^{1}H spectrum without decoupling (4-5 ppm fwhm, Fig. S3).

The 2D ^{27}Al 3QMAS, ^{29}Si{^{1}H} HETCOR, and ^{27}Al{^{29}Si} *J*-HMQC spectra measured at 9.4 T (Supporting Information Figures S5, S7b, and S8) were acquired on a Bruker ASCEND 400 MHz (9.4 T) DNP NMR spectrometer operating at Larmor frequencies of 400.203, 104.283, and 79.501 MHz for ^{1}H, ^{27}Al, and ^{29}Si nuclei, respectively and equipped with a 3.2 mm triple-resonance HXY low-temperature MAS probehead. The 2D ^{27}Al MQMAS spectrum acquired at 9.4 T and 295 K was obtained using a repetition time of 0.2 s for each of 2400 transients, 10 kHz MAS, an incremental t_1 step size of 50 μs, and 50 increments in the indirect isotropic dimension for a total acquisition time of 7 h. The 2D ^{27}Al 3QMAS spectrum acquired at 9.4 T and 93 K was obtained using 960 transients, a repetition time of 1 s, a MAS rate of 10 kHz, an incremental t_1 step size of 50 μs, and 50 increments in the indirect isotropic dimension for a total acquisition time of 13 h. The 2D ^{29}Si{^{1}H} HETCOR spectrum of calcined Si-SSZ-70 was acquired under DNP-NMR conditions as previously reported.[5] The 2D ^{29}Si{^{1}H} HETCOR spectrum of calcined Al-SSZ-70 was acquired using a ^{29}Si{^{1}H} contact time of 0.2 ms, 512 transients, a repetition time of 1.2 s, an incremental t_1 step size of 64 μs, and 32 increments in the indirect ^{1}H dimension for total acquisition time of 5.5 h. Homonuclear ^{1}H-^{1}H eDUMBO-1_{22} decoupling[4] was applied during the ^{1}H evolution periods to improve resolution in the ^{1}H dimensions. For all of the 2D ^{27}Al{^{29}Si} *J*-HMQC spectra, 100 kHz of continuous-wave ^{1}H decoupling was applied during the rotor-synchronized τ delay periods. The signal sensitivity of the 2D ^{27}Al{^{29}Si} *J*-HMQC spectra was enhanced by applying a 1 ms ^{27}Al adiabatic double-frequency sweep (DFS) pulse during the preparation period to invert the ^{27}Al satellite transitions.[6] All of the 2D ^{27}Al 3QMAS spectra were obtained using a 20 μs *z*-filter to eliminate zero-quantum coherences and processed using a shearing transformation to scale the isotropic frequency axes. All of the 1D and 2D spectra, with the exception of the 2D ^{27}Al 3QMAS spectra, were acquired with 100 kHz heteronuclear SPINAL-64 ^{1}H decoupling[7] during the acquisition period. All NMR lineshape simulations and spectral deconvolutions were performed using dmfit software.[8]

Before all NMR measurements, the calcined Al-SSZ-70 sample was stored in a sealed chamber containing a saturated potassium chloride solution to maintain an atmosphere with 85% relative humidity. This was to ensure full hydration of the aluminosilicate framework and maximum NMR visibility (>97%) of ^{27}Al species.[3] To assess for the possibility of highly distorted ^{27}Al species with very large quadrupolar couplings that may not be detected in the ^{27}Al NMR experiments (so-called "NMR-invisible alumina"), ^{27}Al spin-counting measurements were conducted using aluminum nitride (AlN) as an external spin-counting reference. AlN and calcined Al-SSZ-70 samples were loaded into separate 3.2 mm rotors and the sample masses were carefully measured. The fully-relaxed 1D single-pulse ^{27}Al MAS NMR spectra of AlN and Al-SSZ-70 were acquired under the same experimental conditions at 18.8 T, 295 K, 20 kHz MAS, and using a 0.67 μs π/12 pulse for rf excitation. After adjusting for the water content (*ca*. 10 wt% by TGA) and the Si/Al ratio (~25) of the Al-SSZ-70 sample, integration of the 1D ^{27}Al NMR spectra showed that >97% of the ^{27}Al species in calcined Al-SSZ-70 are detected, corroborating that there are no significant extents of NMR-invisible ^{27}Al species.

2. Comparison of ^{29}Si environments in calcined Al- and Si-SSZ-70

Analyses of the 1D ^{29}Si MAS NMR spectra show that the local ^{29}Si framework environments in calcined SSZ-70 are almost identical in the siliceous and aluminosilicate forms. The quantitative 1D single-pulse ^{29}Si NMR spectrum of calcined Si-SSZ-70 (Fig. S1a) exhibits ^{29}Si signals in the Q^4 region at -105 ppm, -110 ppm, -113 ppm, -115 ppm, and -119 ppm from different fully-crosslinked Q^4(0Al) framework ^{29}Si species. The Q^m(*n*Al) notation indicates a tetrahedrally-coordinated Si atom covalently linked through bridging oxygen atoms to *m* other Si or Al atoms, of which *n* are Al. The partially-crosslinked ^{29}Si silanol species at the interlayer channel surfaces give rise to ^{29}Si signals in the Q^3(0Al) region at -97 ppm, -99 ppm, and -101 ppm. These ^{29}Si signals were previously discussed and partially assigned on the basis of dynamic nuclear polarization (DNP-)enhanced solid-state 2D ^{29}Si{^{29}Si} and ^{29}Si{^{1}H} NMR correlation spectra.[5] In the quantitative single-pulse ^{29}Si MAS NMR spectrum of calcined Al-SSZ-70 (Fig. S1b), all of the same ^{29}Si signals are detected, with similar peak positions and linewidths as the spectrum of the siliceous form. The relatively narrow and well-resolved ^{29}Si NMR signals

are consistent with the high crystallinity of Si- and Al-SSZ-70 crystallized in the presence of fluorine as a mineralizing agent, as these materials were.[1] Subtle differences in the relative intensities of the different ^{29}Si signals in the ^{29}Si NMR spectra of Al- and Si-SSZ-70 are attributed to the influences of incorporation of Al heteroatoms into the Al-SSZ-70 framework. Bonding of framework ^{29}Si atoms through bridging oxygen atoms to Al atoms in zeolites is well-known to displace the ^{29}Si NMR signals by +6-7 ppm:[9] a Q^4(1Al) ^{29}Si species at a given T site will exhibit an isotropic ^{29}Si chemical shift that is 6-7 ppm greater than the isotropic ^{29}Si chemical shift of the corresponding Q^4(0Al) ^{29}Si species at the same T site. The ^{29}Si signals at -113 and -115 ppm in the ^{29}Si spectrum of Al-SSZ-70 exhibit diminished relative intensity compared to the ^{29}Si spectrum of Si-SSZ-70, which is attributed to the displacement of ^{29}Si signals from Q^4(1Al) species to higher ppm values. Due to the small absolute quantity of Al in the Al-SSZ-70 material (Si/Al~25[10]) and overlapping ^{29}Si NMR signals from the diversity of Q^4(0Al) and Q^3(0Al) species in SSZ-70, the ^{29}Si signals from Q^4(1Al) species are not resolved and cannot be quantified from the 1D ^{29}Si MAS NMR spectra alone.

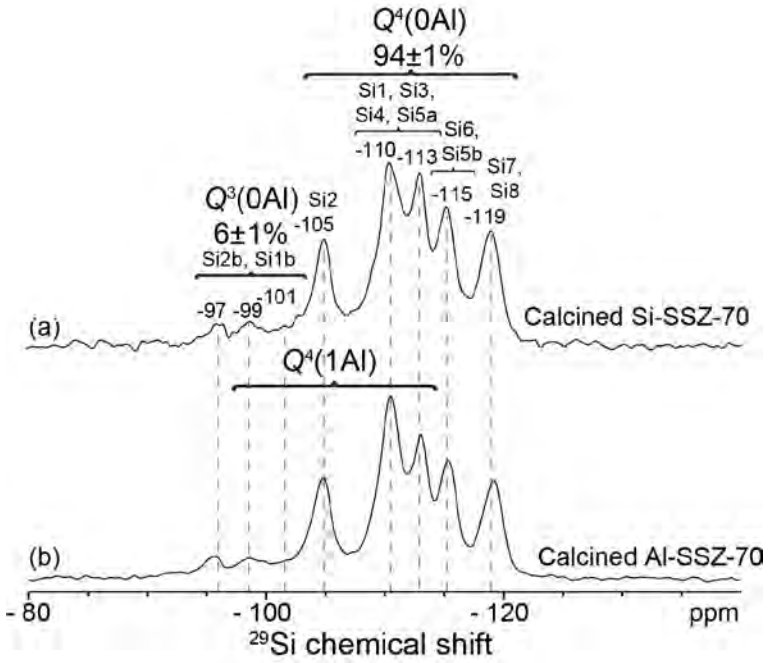

Figure S1. Solid-state 1D quantitative single pulse ^{29}Si MAS NMR spectra of calcined (a) Si-[5] and (b) Al-SSZ-70 acquired at 11.7 T, 298 K, and 12.5 kHz MAS.

3. Enhancement of NMR signal sensitivity under low-temperature measurement conditions

The improved NMR signal sensitivity obtained under low-temperature measurement conditions arises in part from the greater Boltzmann distribution of nuclear spin polarization (M_0) at low temperatures, which is approximately proportional to T^{-1}.[11] Furthermore, thermal noise arises from random electronic fluctuations in the NMR detection coil, reducing signal-to-noise, and is proportional to $T^{-1/2}$.[11] All else being equal, the overall NMR signal-to-noise ratio, S/N, thus has an approximate temperature dependence of $T^{-3/2}$. Measurements conducted at 95 K, such as reported here, may therefore be expected to exhibit *ca*. 5.5x greater signal-to-noise ratios compared to measurements conducted at 295 K. However, the experimental repetition time (interscan delay) is limited by the nuclear spin-lattice (T_1) relaxation times, which tend to increase at lower temperatures, requiring increased experimental times. Fig. S2 shows the fully-relaxed 1D ^{27}Al echo NMR spectra acquired at different temperatures of (a) 93 K and (b) 295 K. At 95 K, a signal-to-noise ratio of ~31 is achieved after only 16 transients (0.5 min experimental time), while at 295 K a lower signal-to-noise ratio of ~15 is achieved after 4 min acquisition time. This demonstrates the substantial time savings (>25x) achieved by using low-temperature acquisition NMR conditions.

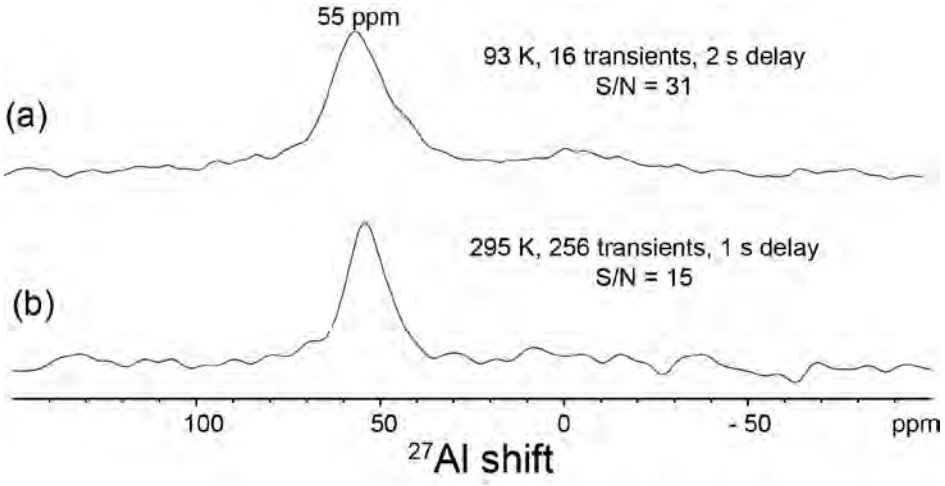

Figure S2. Solid-state 1D ^{27}Al echo NMR spectra of calcined Al-SSZ-70 acquired at 9.4 T, 10 kHz MAS, and (a) 93 K or (b) 295 K.

The ^{27}Al, ^{29}Si, and ^{1}H NMR signals from calcined Al-SSZ-70 exhibit temperature dependent positions and linewidths that are consistent with past results reported for surfactant-templated layered silicates,[12] mesostructured MFI-type zeolite nanosheets,[13] and calcined Si-SSZ-70.[5] For example, the 1D ^{1}H NMR spectrum of calcined Al-SSZ-70 acquired at room temperature (Fig. S3a) exhibits well-resolved signals from isolated Al-OH and/or Si-OH moieties at 2.1-2.8 ppm, adsorbed H_2O at 5.3 ppm, and strongly H-bonded moieties at 7.1-11.5 ppm. These signals indicate that under room temperature conditions, the different ^{1}H species in the hydrated Al-SSZ-70 interlayer regions are relatively mobile. At 95 K and under otherwise identical conditions (Fig. S3b), the ^{1}H NMR signals from adsorbed H_2O and strongly H-bonded –OH moieties broaden substantially (4-5 ppm full-width-half-maximum, fwhm) and are displaced. This broadening manifests in part the inhomogeneous distributions of ^{1}H moieties arising from freezing out of motions of adsorbed water molecules under the low temperature conditions. Interestingly, the ^{1}H signals at 2.4 and 2.8 remain relatively narrow (<1 ppm fwhm), consistent with the assignment of these signals to Si-OH and/or Al-OH moieties that are relatively isolated from adsorbed water molecules or other -OH species.

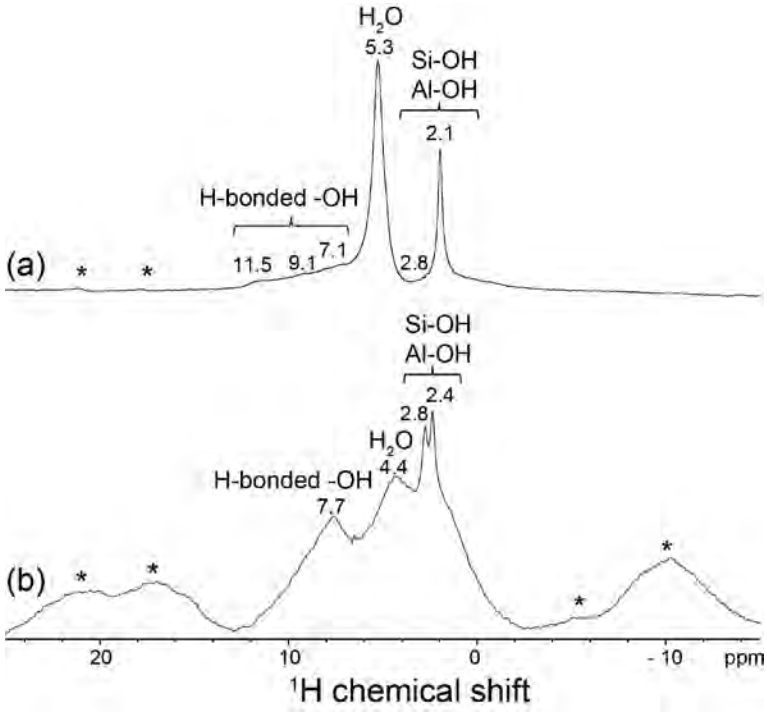

Figure S3. Solid-state 1D (a) single-pulse ^{1}H and (b) ^{1}H echo NMR spectra of calcined Al-SSZ-70 acquired at 18.8 T, 12.5 kHz MAS, and (a) 295 K or (b) 95 K. Asterisks indicate spinning sidebands.

4. Extracting isotropic ^{27}Al chemical shifts from 2D ^{27}Al MQMAS spectra

The ^{27}Al heteroatoms at different T sites in calcined Al-SSZ-70 are expected to exhibit different isotropic ^{27}Al chemical shifts that yield different ^{27}Al NMR signals in the solid-state ^{27}Al NMR spectra, enabling the T site positions and occupancies of the different Al species to be identified. The 1D and 2D ^{27}Al MAS NMR spectra acquired at 18.8 T (Figs. 2, S4, S7, S9, S10a) show well-resolved ^{27}Al signals at 61 ppm, 56 ppm, and 49 ppm (denoted *A, B,* and *C*, respectively) that arise from ^{27}Al atoms in tetrahedrally-coordinated environments, as well as a signal at -2 ppm (denoted *D*) arising from ^{27}Al in octahedrally-coordinated environments. The well-resolved and relatively narrow ^{27}Al signals suggest that the ^{27}Al heteroatoms are preferentially sited at specific T sites in calcined Al-SSZ-70, rather than randomly distributed. The ^{27}Al quadrupolar and chemical shift parameters for the different ^{27}Al species in Al-SSZ-70 are determined by using 2D ^{27}Al triple-quantum MAS (3QMAS) techniques.[14] The 2D ^{27}Al 3QMAS spectra of Al-SSZ-70 (Figs. S4, S5) are presented as 2D contour plots with ^{27}Al signals plotted across MAS and isotropic dimensions on the abscissa and ordinate, respectively, with frequency units of Hz/MHz or ppm. The MAS dimension manifests the same MAS NMR lineshape as detected in conventional 1D ^{27}Al NMR MAS experiments, while the processed indirect dimension reflects only the isotropic contributions to the ^{27}Al signals, with anisotropic broadening effects removed that are associated with second-order quadrupolar interactions.[14] The isotropic chemical shifts, $\delta_{CS,iso}$, are determined for each ^{27}Al signal by fitting the ^{27}Al lineshapes extracted from the 2D MQMAS spectrum.[14] Fig. S4b shows the 1D slices extracted from the 2D MQMAS spectrum at isotropic shifts of 62, 57, 50, and 1.3 ppm (horizontal dotted lines in Fig. S4a), along with simulated ^{27}Al lineshapes for the ^{27}Al signals *A*, *B*, and *C* from tetrahedrally-coordinated ^{27}Al species. The quadrupolar coupling constants C_Q, asymmetry parameters η, and $\delta_{CS,iso}$ values for each ^{27}Al signals, determined by fitting the horizontal ^{27}Al slices extracted from the 2D ^{27}Al 3QMAS spectra, are provided in Table S1.

Isotropic ^{27}Al chemical shifts of tetrahedrally-coordinated ^{27}Al species in aluminosilicate materials correlate linearly to the mean T-O-T bond angle, θ', for a given T site. A commonly applied semi-empirical correlation, developed by Lippmaa, et al,[15,16] relates the ^{27}Al isotropic chemical shift to the mean -Al-O-Si-bond angle for a given T site:

$$\delta_{\mathrm{CS,iso}} = -0.5\theta' + 132\ (\mathrm{ppm}) \qquad \text{(Eqn. S1)}$$

This equation relies on the average T site geometry obtained from powder diffraction measurements, which are not always representative of the local geometry around Al sites that make up a small fraction of the overall number of T sites.[17] Nevertheless, it provides a reasonable approximation for high-silica zeolites with mean -Al-O-Si- bond angles less than 180 degrees[18] such as Al-SSZ-70 (Si/Al ~ 25), and provides an additional constraint on the assignments of the different ^{27}Al signals in the ^{27}Al NMR spectra of Al-SSZ-70. The predicted isotropic ^{27}Al chemical shifts, calculated from the known structure of calcined Si-SSZ-70 and Eqn. S1, are tabulated in Table S2, shown alongside the corresponding T sites in the schematic diagram in Fig. S6a, and compared with the experimentally-determined $\delta_{CS,iso}$ values for ^{27}Al signals *A, B,* and *C* in Fig. S4b. On the basis of this comparison, ^{27}Al signal *A* at $\delta_{CS,iso}$ = 62 ppm is assigned to ^{27}Al species in fully-crosslinked T2a and T2b sites, which have predicted $\delta_{CS,iso}$ values of 61 ppm. ^{27}Al signal *B* at $\delta_{CS,iso}$ = 57 ppm is assigned to ^{27}Al species at T3 and/or T5a sites, which have calculated $\delta_{CS,iso}$ values of 58 and 57 ppm, respectively. Signal *C* at $\delta_{CS,iso}$ = 50 ppm is tentatively assigned to ^{27}Al atoms in T5b sites (predicted to be at 53 ppm), though the agreement between the predicted and experimental ^{27}Al $\delta_{CS,iso}$ values is relatively poor. Further confidence in the assignments of ^{27}Al signals *A*-*C* are provided by complementary analyses of 2D ^{27}Al MQMAS spectra acquired at different magnetic field strengths and temperatures, shown in Fig. S5. At lower magnetic field strengths (9.4 T) the ^{27}Al signals are modestly displaced and broadened by comparison to the spectra obtained at 18.8 T due to the greater contribution of quadrupolar broadening at the lower magnetic field strength. At decreased temperatures (<95 K), the ^{27}Al signals are broadened further in both the MAS and isotropic dimensions, consistent with inhomogeneous temperature-dependent broadening effects, as discussed in Section 3 above.

Elucidating the nature of the octahedrally-coordinated ^{27}Al species that give rise to ^{27}Al signal *D* is more challenging, as octahedrally-coordinated ^{27}Al species in zeolite frameworks are rare, though may arise as products of partial reversible dealumination combined with hydration effects.[18] Signal *D* could also be attributed to extra-framework alumina species such as residual alumina gel remaining in the material after the hydrothermal synthesis and calcination. However, though signal *D* is relatively broad in the MAS dimension of the 2D ^{27}Al MQMAS spectrum, this broadening arises primarily from anisotropic quadrupolar interactions, as evidenced by the relatively narrow linewidth (2 ppm full-width half-maximum, FWHM) associated with the signal in the isotropic dimension in Fig. S4a. This indicates that signal *D* arises from a narrow distribution of ^{27}Al species in non-symmetric environments, which is typically not the case for extra-framework alumina species. The ^{27}Al lineshape of signal *D* is simulated using a Czjzek lineshape,[19] which is characteristic of a distribution of ^{27}Al quadrupolar parameters as previously observed in aluminosilica glasses[20] or aluminosilicate zeolites with non-ordered Al distributions.[21] The 2D ^{27}Al{^{29}Si} through-bond-mediated NMR correlation spectra and analyses discussed below provide further evidence that the ^{27}Al signal in the octahedral region is associated with ^{27}Al species that are covalently linked to fully-condensed ^{29}Si species and are therefore located within the aluminosilicate zeolite framework.

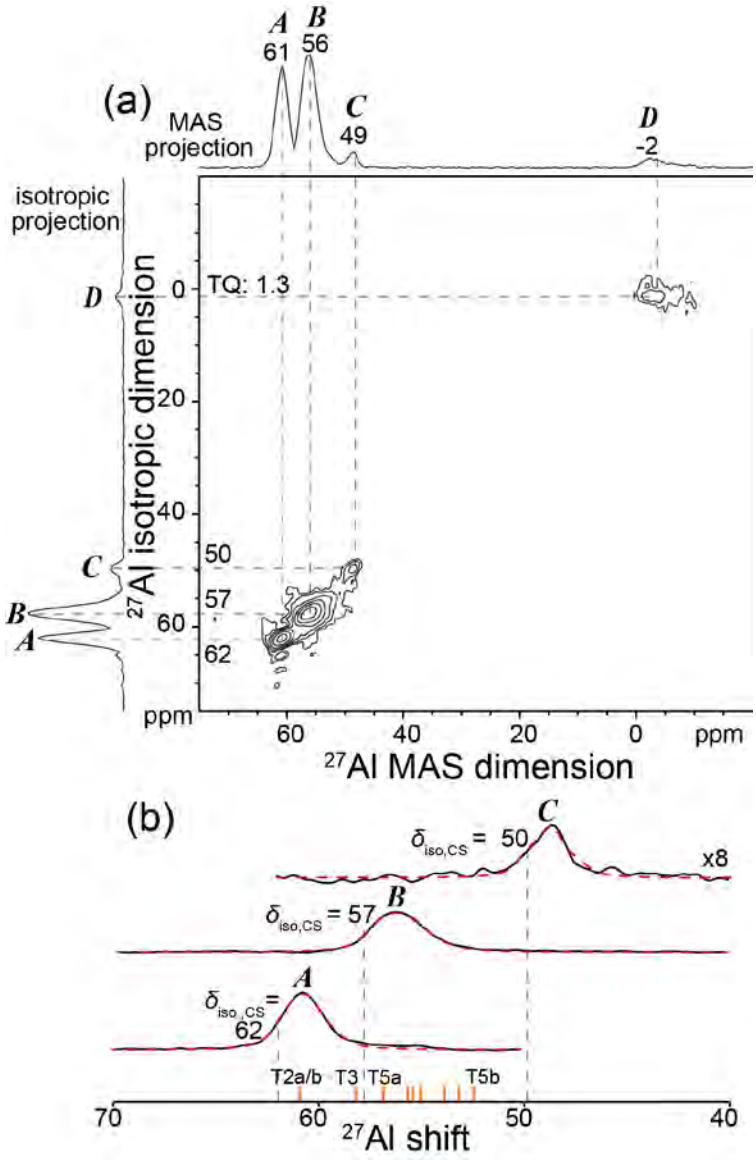

Figure S4. (a) Solid-state 2D triple-quantum (3Q) MAS ^{27}Al NMR spectrum of calcined Al-SSZ-70 acquired at 18.8 T, 298 K, and 35 kHz MAS, with MAS and isotropic projections shown along the horizontal and vertical axes, respectively. Horizontal cross-sections at isotropic shifts of 50, 58, and 62 ppm are extracted from the 2D ^{27}Al 3QMAS spectrum and shown in (b). The red dotted lines are simulations of the ^{27}Al lineshapes obtained using the parameters listed in Table 1 and the orange lines are predicted ^{27}Al isotropic chemical shifts for ^{27}Al heteroatoms sited at each of the different T sites in Al-SSZ-70, calculated using Eqn. S1.

Table S1. ^{27}Al quadrupolar parameters and isotropic chemical shifts for calcined Al-SSZ-70[a]

^{27}Al signal:	*A*	*B*	*C*	*D*
$\delta_{CS,iso}$ (ppm)	62	57	50	1.3
C_Q (MHz)	2.2	3.0	2.4	5.5[c]
η[b]	0.5	0	0.6	-[c]

[a] Extracted from analysis of the 2D ^{27}Al 3QMAS spectrum in Fig. S2.

[b] The fits of the ^{27}Al NMR lineshapes were found to be generally insensitive to the asymmetry parameter η, similar to previous ^{27}Al 3QMAS NMR analyses of aluminosilicate zeolites.[22]

[c] The ^{27}Al signal *D* in the six-coordinate region was fitted by using a single quadrupolar Czjzek lineshape, which reflects a distribution of quadrupolar parameters characterized by a maximum C_Q value of 5.5 MHz.

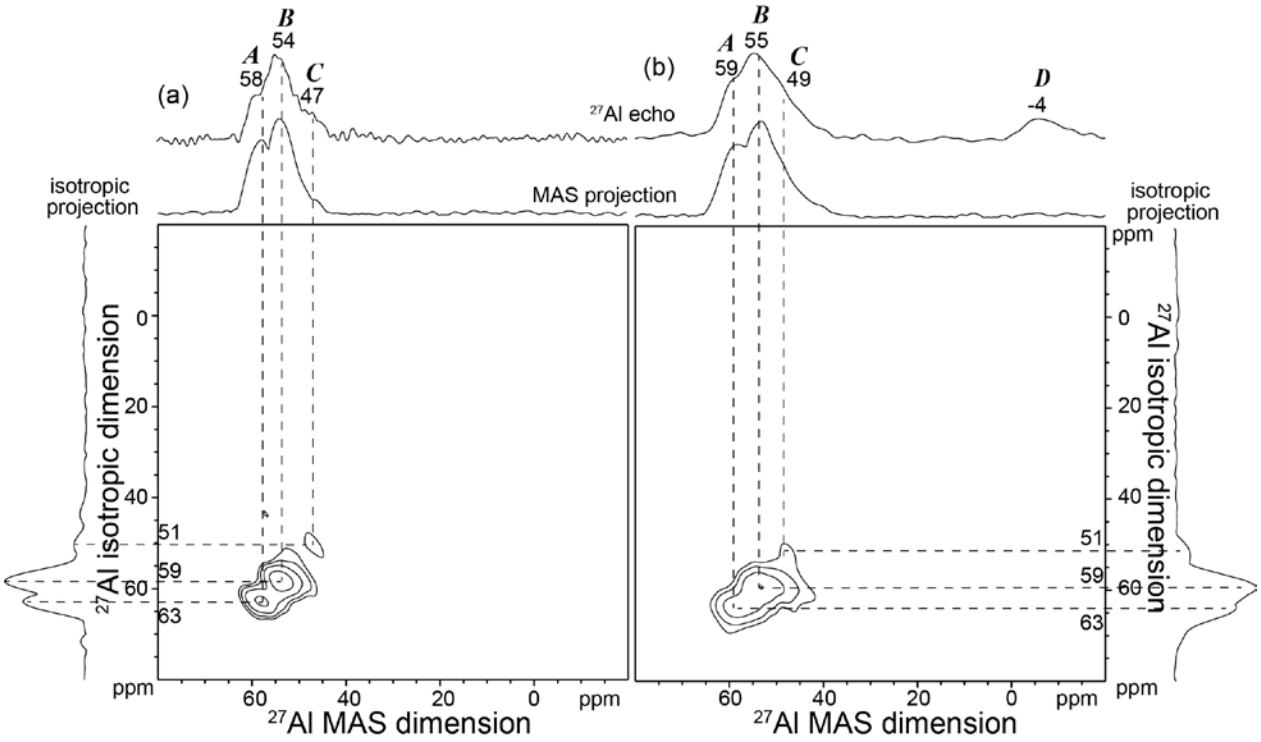

Figure S5. Solid-state 2D 3QMAS ^{27}Al NMR spectra of calcined Al-SSZ-70 acquired at 9.4 T, 10 kHz MAS, and (a) 298 K or (b) 93 K. Solid-state 1D ^{27}Al echo MAS NMR spectra acquired under the same conditions are shown along the horizontal axes for comparison with the MAS projections, and the isotropic projections are shown along their respective vertical axes.

Table S2. Predicted ^{27}Al isotropic chemical shift values $\delta_{CS,iso}$ for ^{27}Al atoms at each T site in Al-SSZ-70[a]

T-site	^{27}Al $\delta_{CS,iso}$ (ppm)
1a	56
1b	-[b]
2a	61
2b	61[c]
3	58
4a	55
4b	55
5a	57
5b	52
6	53
7a	53
7b	55
8a	55
8b	54

[a] Calculated using the mean -T-O-T- angles for each T site from the structure of calcined Si-SSZ-70[5] and Eqn. S1.

[b] T1b is a partially-crosslinked site protruding into the interlayer channels of calcined Al-SSZ-70 and is associated with at least one hydroxyl group. Eqn. S1 does not account for Al-OH bonds, which are expected to influence the ^{27}Al isotropic shifts.

[c] T2b may be either completely- or partially- crosslinked. This value is for completely-crosslinked Al2b sites.

5. Assignment of the correlated signals in the 2D ^{27}Al{^{29}Si} J-HMQC spectra

The different correlated ^{27}Al-^{29}Si signals in the 2D ^{27}Al{^{29}Si} *J*-mediated spectra (Figs. 2a, S7) are assigned based on comparisons with previous 2D ^{29}Si{^{29}Si} and ^{29}Si{^{1}H} NMR analyses of calcined Si-SSZ-70,[5] analyses of 2D ^{27}Al MQMAS spectra (Figs. S4, S5), well-established semi-empirical correlations relating the isotropic ^{27}Al and ^{29}Si chemical shift values to the mean -T-O-T- bond angles and T-O bond lengths,[15,23–26] and prior literature.[9,27] Fig. S7 shows a comparison of the 2D ^{27}Al{^{29}Si} *J*-HMQC spectra of Al-SSZ-70 acquired at 18.8 T and 95 K (b, same spectrum as Fig. 2a) and at 9.4 T and 91 K (b), both of which exhibit all of the same correlated signal intensities but with ^{27}Al signals that are modestly broadened and displaced in (b) because of the larger contribution from 2nd-order quadrupolar interactions at the lower magnetic field strengths. Correlated ^{27}Al-^{29}Si signals are resolved in the 2D *J*-HMQC spectra at ^{29}Si shifts of -107, -105, and -101 to -99 ppm. These are assigned to different Q^4(1Al) ^{29}Si species by comparison of the experimental Q^4(1Al) ^{29}Si chemical shifts to values calculated using a well-established semi-empirical correlation relating the Q^4(1Al) ^{29}Si chemical shift, δ, to the average -T-O-T- bond angles, θ':[23,24]

$$\delta = 151 - 266 \sin\left(\frac{\theta'}{2}\right) \text{ (ppm)} \qquad \text{(Eqn. 2)}$$

The Q^4(1Al) ^{29}Si isotropic chemical shift values calculated for each T site in Al-SSZ-70 are tabulated in Table S3 and shown alongside the corresponding T sites in the schematic diagram in Fig. S6a. Based on these values, the Q^4(1Al) ^{29}Si signals at -101 ppm resolved in the 2D ^{27}Al{^{29}Si} *J*-HMQC spectra arises from Q^4(1Al) Si2a/Si2b, while those at -105 ppm manifest overlapping ^{29}Si signal contributions from Q^4(1Al) Si1a and Si3. The Q^4(1Al) signals at -107 ppm may arise from Q^4(1Al) Si4a,4b,5a,6,7b, and/or 8a, but can be assigned more precisely on the basis of the correlated signal intensities in the 2D ^{27}Al{^{29}Si} spectra and the ^{27}Al MQMAS analyses. The ^{27}Al signal at 55 ppm is correlated with ^{29}Si signals at -99 to -101 ppm from Q^4(1Al) Si2, consistent with its assignment to Al3 as discussed above. Al3 species are expected to be covalently linked (through bridging oxygen atoms) to Si6 species, and so the correlated ^{27}Al-^{29}Si signal at -107 ppm in the ^{29}Si dimension and 55 ppm in the ^{27}Al dimension is assigned to Al3-O-Si6 moieties. From the ^{27}Al MQMAS analyses discussed above, the ^{27}Al signal at $\delta_{CS,iso}$ = 50 ppm most likely arises from Al5b species, consistent with the assignment of the correlated ^{27}Al-^{29}Si signal at -107 ppm in the ^{29}Si dimension and 49 ppm in the ^{27}Al dimension to Al5b-O-Si4b and Al5b-O-Si7b moieties. Fig. S6a shows a structural diagram of the calcined Al-SSZ-70 structure with each T site labelled with the associated isotropic ^{27}Al (red) and Q^4(1Al) ^{29}Si (blue) chemical shifts predicted from Eqn. S1 and S2. For comparison, Fig. S6b shows the experimental isotropic ^{27}Al and Q^4(1Al) ^{29}Si chemical shifts extracted from the NMR analyses for each T site partially occupied by ^{27}Al and/or Q^4(1Al) ^{29}Si atoms. The comparison shows that the agreement between predicted and experimental isotropic chemical shifts is very good, within 1-2 ppm for all of the ^{27}Al and ^{29}Si species.

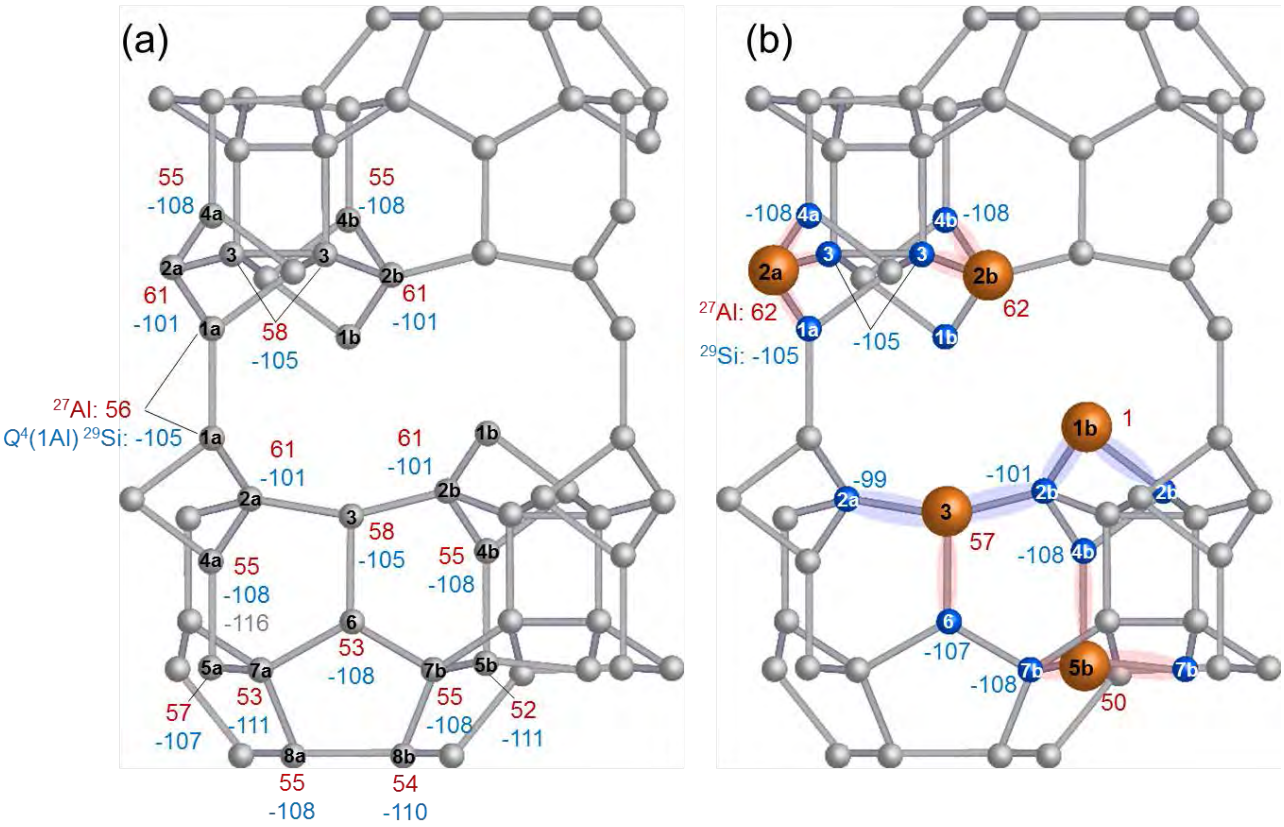

Figure S6. Schematic diagrams of the structures of calcined Al-SSZ-70 (a) indicating the isotropic ^{27}Al (red) and ^{29}Si (blue) chemical shifts for ^{27}Al or Q^4(1Al) ^{29}Si species in each T site predicted from Eqns. S1 or S2; and (b) with the isotropic ^{27}Al (red) and ^{29}Si (blue) chemical shifts (in ppm) determined experimentally from the NMR analyses in Fig. 2 and S4,S5,S7. The atoms labeled are those pertinent to the discussion in the main manuscript, with orange spheres in (b) indicating the five T sites that are partially occupied by Al atoms and the small blue spheres indicating the 10 T sites partially occupied by Q^4(1Al) Si atoms. The remaining grey spheres represent T sites occupied by Q^4(0Al) Si atoms that are not directly bonded to framework Al atoms; their ^{29}Si isotropic chemical shifts have been omitted for reasons of clarity but are reported in ref. [5].

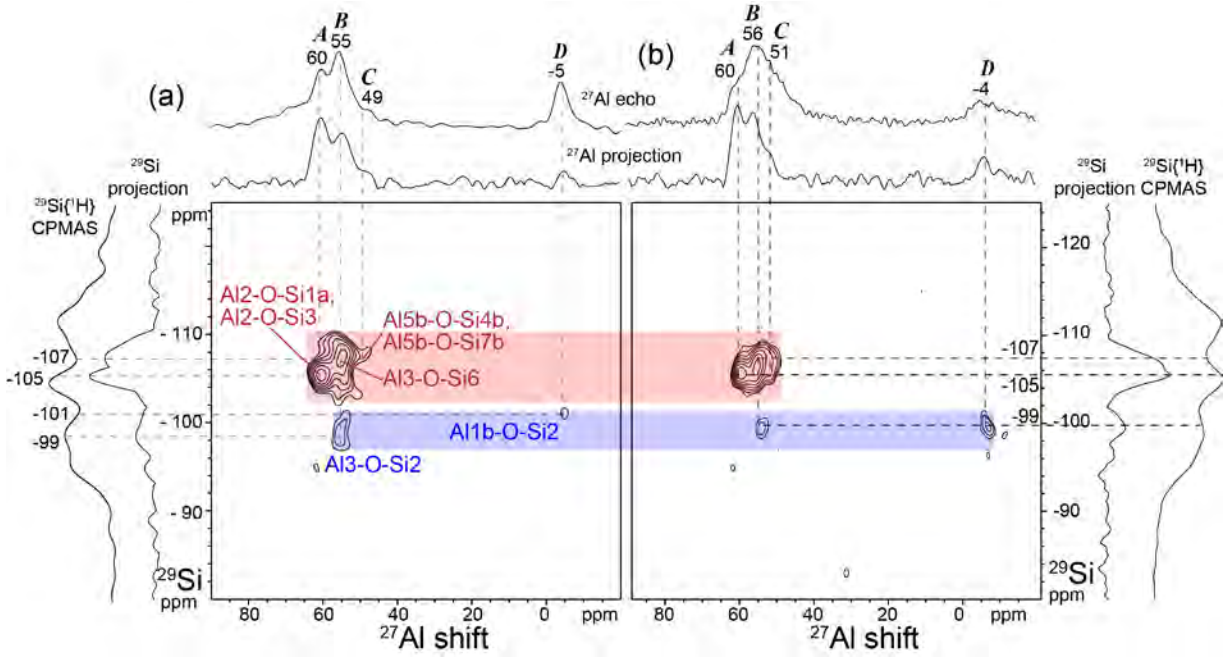

Figure S7. Solid-state 2D ^{27}Al{^{29}Si} *J*-mediated NMR correlation spectra of calcined Al-SSZ-70 acquired at (a) 18.8 T, 12.5 kHz MAS, and 97 K (same spectrum as Figure 2a) and (b) 9.4 T, 8 kHz MAS, and 91 K. Solid-state 1D ^{27}Al echo and ^{29}Si{^{1}H} CPMAS spectra acquired under the same conditions are shown along the corresponding axes for comparison with the 1D projections of the 2D spectra.

Table S3. Predicted ^{29}Si isotropic chemical shift values δ for Q^4(1Al) ^{29}Si atoms in each T site in Al-SSZ-70

T-site	Q^4(1Al) ^{29}Si δ (ppm)
1a	-105
1b	-[a]
2a	-101
2b	-101[b]
3	-105
4a	-108
4b	-108
5a	-107
5b	-111
6	-108
7a	-111
7b	-108
8a	-108
8b	-110

[a] T1b is a partially-crosslinked site protruding into the interlayer channels of calcined Al-SSZ-70 and is associated with at least one hydroxyl group. Eqn. 2 does not account for Si-OH bonds, which are known to influence the ^{29}Si isotropic shifts.

[b] T2b may be either completely- or partially- crosslinked. The reported value is for completely-crosslinked Si2b sites.

6. Hydration environments in calcined Si- and Al-SSZ-70

The different partially-crosslinked T sites in the interlayer channel regions of calcined SSZ-70 are associated with -OH groups with different extents of hydrogen bonding that yield correlated ^{29}Si{^{1}H} or ^{27}Al{^{1}H} signal intensities in the 2D ^{29}Si{^{1}H} and ^{27}Al{^{1}H} HETCOR spectra in Figs. 2b and S8. For example, the 2D ^{29}Si{^{1}H} HETCOR spectrum of calcined Si-SSZ-70 in Fig. S8a (acquired under DNP-NMR conditions, see ref. [5]) shows ^{29}Si signals in the -96 to -99 ppm range from partially-crosslinked Q^3(0Al) ^{29}Si species that are correlated with ^{1}H signals at 3.0 ppm (green shaded region), 7.0 ppm, and 8.8 ppm (red shaded region), which arise respectively from isolated Si-OH moieties, DNP solvent molecules, and nests of H-bonded Si-OH species.[5] Partially resolved ^{29}Si signals in the -105 to -112 ppm range arise from fully-crosslinked Q^4 species in the Si-SSZ-70 zeolite framework. By comparison, the 2D ^{29}Si{^{1}H} HETCOR spectrum of calcined Al-SSZ-70 (Fig. S8b) shows correlated signal intensities at ^{29}Si chemical shifts of -98 to -102 ppm from Q^3(0Al) species that are correlated to ^{1}H signals from isolated -OH groups in the 0-3.7 ppm range and from H-bonded -OH groups in the 7.6 to 11.1 ppm range. Additional correlated signal intensities at ^{29}Si chemical shifts of -104 to -114 ppm arise from overlapping ^{29}Si signals from fully-crosslinked Q^4(0Al) and Q^4(1Al) species, while the broad correlated signals at 6.9 ppm in the ^{1}H dimension and -98 to -107 ppm in the ^{29}Si dimension (grey shade dregion) are attributed to interactions of adsorbed water molecules and framework ^{29}Si species. The relatively low signal-to-noise ratio (S/N ~ 3) of the 2D ^{29}Si{^{1}H} HETCOR spectrum precludes more detailed analysis of the spectrum and is likely due to the low density of ^{1}H species and the inhomogeneously-broadened ^{29}Si and ^{1}H signals. Despite the low sensitivity, the resolution of the 2D ^{29}Si{^{1}H} HETCOR spectrum is sufficient to determine that different types of isolated and strongly H-bonded -OH species are present in calcined Al-SSZ-70, similar to its siliceous analogue.

We note that in the 2D ^{27}Al{^{1}H} HETCOR spectrum in Fig. 2b, there are no detectable ^{27}Al-^{1}H intensity correlations from tetrahedrally-coordinated ^{27}Al species and strongly H-bonded -OH (^{1}H shifts >7.5 ppm). This suggests that few of the tetrahedrally-coordinated ^{27}Al species are located at partially-crosslinked Al2b sites, which are expected to be associated with nests of strongly H-bonded hydroxyl moieties.

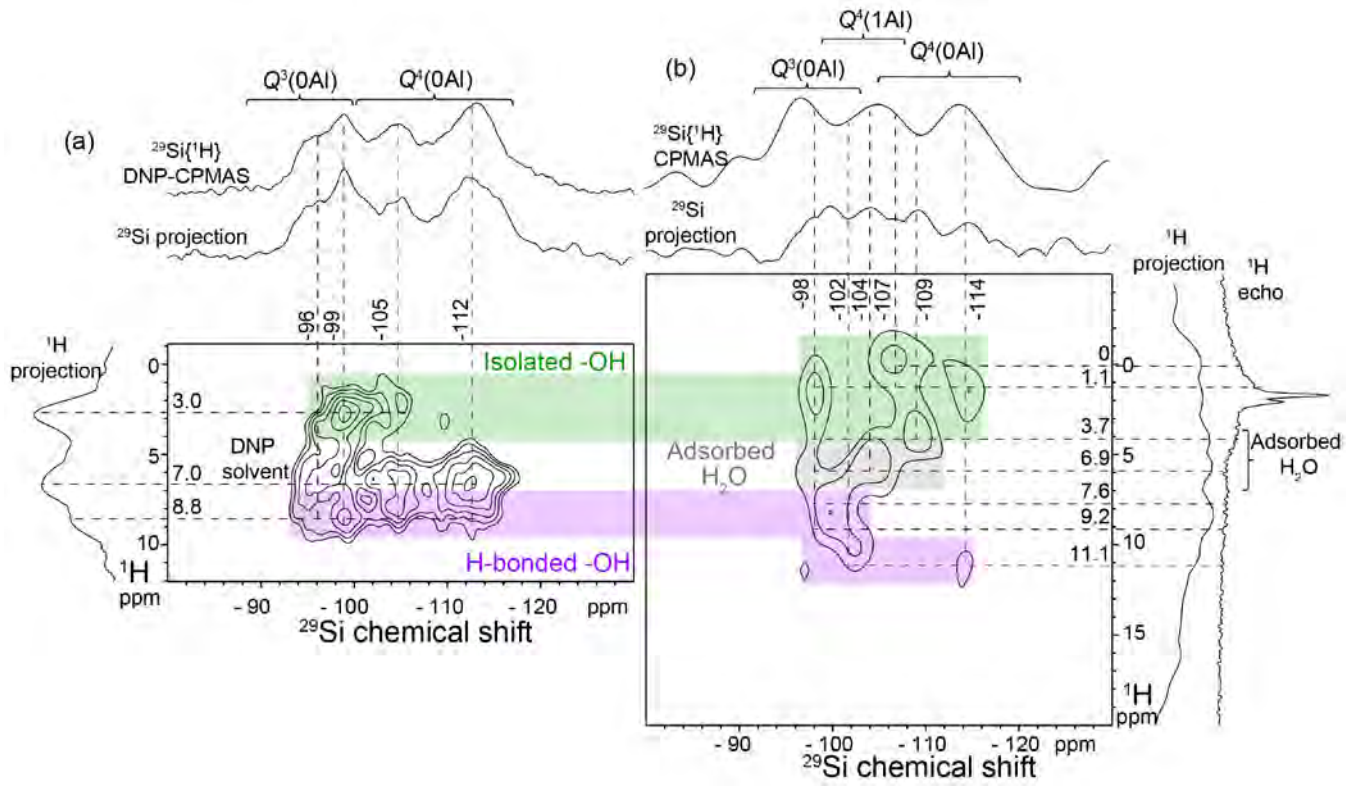

Figure S8. Solid-state 2D ^{29}Si{^{1}H} HETCOR spectra of calcined (a) Si-SSZ-70 and (b) Al-SSZ-70. Solid-state 1D ^{29}Si{^{1}H} CPMAS or ^{1}H echo spectra are shown along the horizontal or vertical axes, respectively, for comparison with the 1D projections of the 2D spectra. The spectra in (a) were acquired under DNP-NMR conditions at 9.4 T, 10 kHz MAS, 95 K, with ^{29}Si{^{1}H} contact time of 0.2 ms, in the presence of 16 mM TEKPol biradical in TCE (DNP solvent), and under 263 GHz microwave irradiation (adapted from Ref. [5]). The spectra in (b) were acquired under low-temperature NMR conditions of 9.4 T, 10 kHz MAS, 93 K, and with ^{29}Si{^{1}H} contact times of 0.2 ms.

7. Al occupancies at each T site in calcined Al-SSZ-70

The relative populations of the different ^{27}Al species in calcined Al-SSZ-70 are quantified by deconvolution of the 1D single-pulse ^{27}Al spectrum in Fig. S9a. The positions of each of the 5 T sites that occupied by Al are shown in the schematic structures of calcined Al-SSZ-70 in Figs. S6b and S9b. All of the ^{27}Al signals detected are assigned to ^{27}Al species within the Al-SSZ-70 framework, with no evidence for extra-framework species. The ^{27}Al spectrum was simulated using the spectral parameters for each ^{27}Al signal given in Table S2. Based on the relative integrated intensities of the ^{27}Al signals in the quantitative 1D single-pulse ^{27}Al spectrum and the structure of calcined SSZ-70,[5,28] the Al/T occupancies of each T site in calcined Al-SSZ-70 are determined and reported in Table S4. Notably, T1b, T2a/b, and T3 are all located at the surfaces of the interlayer channels, while T5b is located at the surfaces of the intralayer **MWW**-type channels.

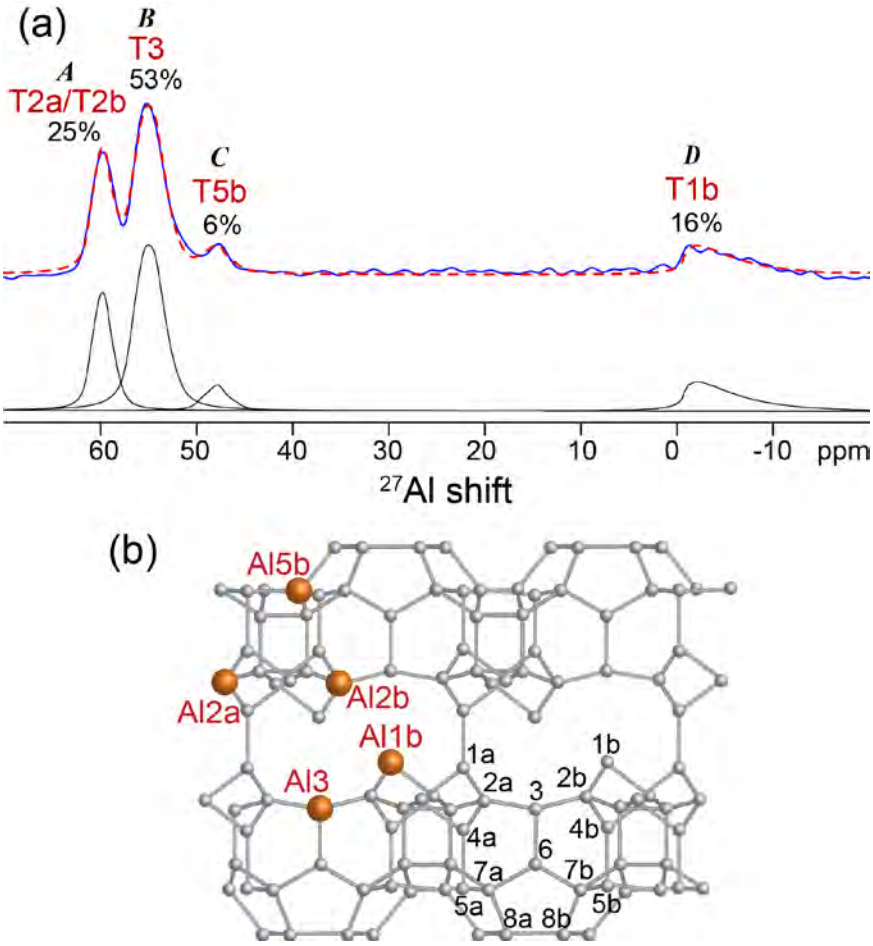

Figure S9. (a) Solid-state single-pulse 1D ^{27}Al MAS NMR spectrum of calcined Al-SSZ-70, acquired at 18.8 T, 35 kHz MAS, and 295 K. The red dotted line is a simulation of the total spectrum, based on deconvolutions of the individual signals, as shown offset below. (b) Schematic diagram of the framework structure of Al-SSZ-70 (same as Fig. 2c), with orange indicating the T sites that are occupied by Al heteroatoms as determined by the solid-state NMR analyses.

Table S4. Al/T fractional occupancies in Al-SSZ-70

T site	Al/T
T1b	0.35
T2a/b[a]	0.09
T3	0.19
T5b	0.13

[a] Al2a and Al2b sites are structurally very similar and their respective ^{27}Al NMR signals are not resolved.

8. Comparison of calcined and as-made Al-SSZ-70

The analyses presented here of calcined Al-SSZ-70 are expected to provide additional structural constraints for future studies of the as-made analogue, the interlayer structure of which has been elusive and is still not known. The framework locations of the Al heteroatoms in Al-SSZ-70 are not expected to change substantially upon calcination, though their coordination might. The 1D ^{27}Al spectra of calcined and as-made Al-SSZ-70 are compared in Fig. S10. The ^{27}Al spectrum of as-made Al-SSZ-70 shows a narrow signal at 56 ppm with a shoulder at 50 ppm, likely arise respectively from Al3 and Al5b sites, which are not expected to change substantially on calcination. No ^{27}Al signal at 60 ppm from Al2a/Al2b sites is detected, suggesting that these species may arise in calcined Al-SSZ-70 as a result of the calcination process. The ^{27}Al spectrum of as-made Al-SSZ-70 additionally

shows a broad ^{27}Al signal at 5 ppm, which arises from octahedrally-coordinated ^{27}Al species. This is consistent with the presence of octahedrally-coordinated framework Al species in both calcined and as-made Al-SSZ-70. We expect a more detailed solid-state NMR analysis of as-made SSZ-70 to be the subject of a future manuscript.

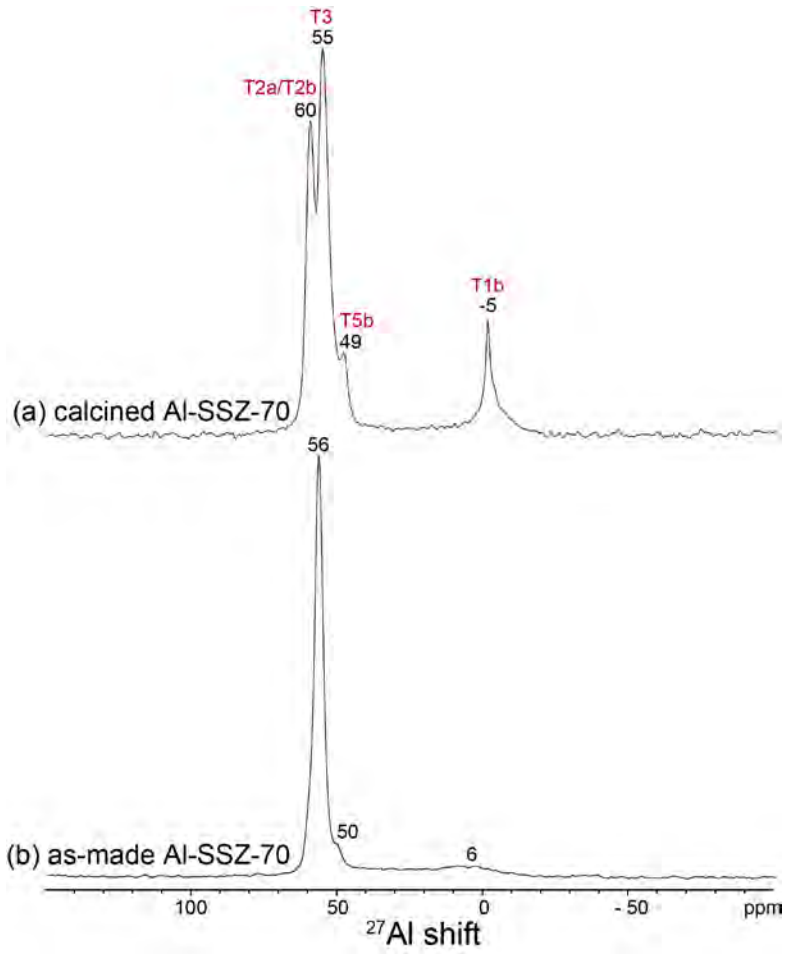

Figure S10. Solid-state 1D ^{27}Al echo MAS NMR spectra of (a) calcined and (b) as-made Al-SSZ-70 acquired at 18.8 T, 295 K, and (a) 35 or (b) 20 kHz MAS.

9. Additional references

[1] R. H. Archer, S. I. Zones, M. E. Davis, *Microporous Mesoporous Mater.* **2010**, *130*, 255–265.

[2] A. Bergamaschi, A. Cervellino, R. Dinapoli, F. Gozzo, B. Henrich, I. Johnson, P. Kraft, A. Mozzanica, B. Schmitt, X. Shi, *J. Synchrotron Radiat.* **2010**, *17*, 653–668.

[3] L. Mafra, J. A. Vidal-Moya, T. Blasco, *Structural Characterization of Zeolites by Advanced Solid State NMR Spectroscopic Methods*, **2012**.

[4] B. Elena, G. de Paëpe, L. Emsley, *Chem. Phys. Lett.* **2004**, *398*, 532–538.

[5] S. Smeets, Z. J. Berkson, D. Xie, S. I. Zones, W. Wan, X. Zou, M. F. Hsieh, B. F. Chmelka, L. B. McCusker, C. Baerlocher, *J. Am. Chem. Soc.* **2017**, *139*, 16803–16812.

[6] E. Van Veenendaal, B. H. Meier, A. P. M. Kentgens, *Mol. Phys.* **1998**, *93*, 195–213.

[7] B. M. Fung, A. K. Khitrin, K. Ermolaev, *J. Magn. Reson.* **2000**, *142*, 97–101.

[8] D. Massiot, F. Fayon, M. Capron, I. King, S. Le Calvé, B. Alonso, J. O. Durand, B. Bujoli, Z. Gan, G. Hoatson, *Magn. Reson. Chem.* **2002**, *40*, 70–76.

[9] N. Kodakari, K. Tomita, K. Iwata, N. Katada, M. Niwa, *Langmuir* **1998**, *14*, 4623–4629.

[10] R. H. Archer, J. R. Carpenter, S.-J. Hwang, A. W. Burton, C.-Y. Chen, S. I. Zones, M. E. Davis, *Chem. Mater.* **2010**, *22*, 2563–2572.

[11] P. Styles, N. F. Soffe, C. A. Scott, D. A. Cragg, F. Row, D. J. White, P. C. J. White, *J. Magn. Reson.* **1984**, *60*, 397–404.

[12] S. Cadars, N. Mifsud, A. Lesage, J. D. Epping, N. Hedin, B. F. Chmelka, L. Emsley, *J. Phys. Chem. C* **2008**, *112*, 9145–9154.

[13] Z. J. Berkson, R. J. Messinger, K. Na, Y. Seo, R. Ryoo, B. F. Chmelka, *Angew. Chem. - Int. Ed.* **2017**, *56*, 5164–5169.

[14] L. Frydman, D. M. Grant, R. K. Harris, *Encycl. Nucl. Magn. Reson. Vol. 9 Adv. NMR* **2002**, *9*, 262–274.

[15] E. Lippmaa, A. Samoson, M. Magi, *J. Am. Chem. Soc.* **1986**, *108*, 1730–1735.

[16] A. Samoson, E. Lippmaa, G. Engelhardt, U. Lohse, H. G. Jerschkewitz, *Chem. Phys. Lett.* **1987**, *134*, 589–592.

[17] J. Dědeček, Z. Sobalík, B. Wichterlová, *Catal. Rev. - Sci. Eng.* **2012**, *54*, 135–223.

[18] J. A. Van Bokhoven, D. C. Koningsberger, P. Kunkeler, H. Van Bekkum, A. P. M. Kentgens, *J. Am. Chem. Soc.* **2000**, *122*, 12842–12847.

[19] J. B. d'Espinose de Lacaillerie, C. Fretigny, D. Massiot, *J. Magn. Reson.* **2008**, *192*, 244–251.

[20] G. Le Caër, B. Bureau, D. Massiot, *J. Phys. Condens. Matter* **2010**, *22*, 065402.

[21] P. Klein, V. Pashkova, H. M. Thomas, S. R. Whittleton, J. Brus, L. Kobera, J. Dedecek, S. Sklenak, J. Heyrovsky, *J. Phys. Chem. C* **2016**, *120*, 14216–14225.

[22] C. A. Fyfe, J. L. Bretherton, L. Y. Lam, *J. Am. Chem. Soc.* **2001**, *123*, 5285–5291.

[23] S. Ramdas, J. Klinowski, *Nature* **1984**, *308*, 521–523.

[24] G. Engelhardt, S. Luger, J. C. Buhl, J. Felsche, *Zeolites* **1989**, *9*, 182–186.

[25] Y. Liu, H. Nekvasil, J. Tossell, *J. Phys. Chem. A* **2005**, *109*, 3060–3066.

[26] D. M. Dawson, R. F. Moran, S. E. Ashbrook, *J. Phys. Chem. C* **2017**, *121*, 15198–15210.

[27] M. A. Camblor, A. Corma, M.-J. Díaz-Cabañas, C. Baerlocher, *J. Phys. Chem. B* **1998**, *102*, 44–51.

[28] C. Baerlocher, L. B. McCusker, "Database of Zeolite Structures," can be found at http://www.iza-structure.org/databases/, which is regularly updated.